Characterization of Special Fibers and Fiber Devices

S. B. POOLE, J. E. TOWNSEND, D. N. PAYNE, M. E. FERMANN, G. J. COWLE, R. I. LAMING, AND P. R. MORKEL

(*Invited Paper*)

Abstract—**Recent developments in specialist fibers for device applications has resulted in simultaneous progress in measurement techniques to characterize these fibers but, while there is much literature concerning such fibers and devices, few papers directly address the measurement problems. Methods developed to characterize birefringent fibers (both those with high circular or linear birefringence and those with negligible intrinsic birefringence) are presented and their relative merits discussed. Fibers with high nonlinear coefficients exhibit interesting optical phenomena and methods have been developed to determine second harmonic, Pockels and Kerr effects, parametric phenomena and the Verdet constant of silica and higher loss, nonsilica fibers. Fibers containing rare-earth ions are of interest both as active (laser and amplifiers) and passive systems. Not only have techniques been developed to characterize these devices but also conventional methods have been modified to quantify dopant parameters within the fiber. Techniques for the measurement of the diverse properties of all these different fibers are presented with results and, where appropriate, the problems with their characterization are discussed.**

I. Introduction

OPTICAL fibers are making ever-increasing inroads into areas traditionally satisfied by older, more established technologies. One of the prime vehicles for this trend is the proliferation of specially tailored fibers designed for specific applications [1]. Since these applications are diverse (especially in the sensor field [1]) and the required fiber characteristics often subtle, measurement of the fiber response frequently presents a challenge. On occasions it is even necessary to resort to indirect measurements by observing the performance of the fiber in the intended application, from which its characteristics can be implied. A particular example here is the fiber gyroscope, where signal-processing techniques have progressed to such an extent that the gyro itself provides the ideal environment for high-accuracy measurements of fiber polarizer performances [2].

While there is much literature concerning special fibers and their applications, there have, to date, been few papers which directly address the measurement problems posed by these fibers [3]. This paper attempts to redress this balance and provides an overview of the techniques and remaining problems in this extremely important area.

To keep the paper to a reasonable length, a working knowledge of measurements of single-mode fibers is assumed, and only areas where the required measurements differ from those for single-mode fibers are discussed in detail. For instance, the techniques for fiber refractive-index profiling are applicable for both "standard" and "special" fibers and so are not discussed here.

Manuscript received February 16, 1989; revised April 28, 1989.

S. B. Poole was with the Optical Fibre Group, Department of Electronics and Computer Science, University of Southampton, Hants., U.K. He is now with the Optical Fibre Technology Centre, University of Sydney, Sydney, NSW, 2006 Australia.

J. E. Townsend, D. N. Payne, G. J. Cowle, R. I. Laming, and P. R. Morkel are with the Optical Fibre Group, Department of Electronics and Computer Science, University of Southampton, Hants., U.K.

M. E. Fermann was with the Optical Fibre Group, Department of Electronics and Computer Science, University of Southampton, Hants., U.K. He is now with the Institut fur Allgemeine, Electrotechnik und Electronik, Vienna, Austria.

IEEE Log Number 8929124.

II. Birefringent Fibers

A. Ultralow Birefringence Fibers

Fibers with negligible internal birefringence are made by rotating the preform of a conventional fiber about its longitudinal axis during fiber drawing [4] so as to impart a permanent twist to the fiber. As a consequence of the rapid rotation of the fiber birefringence axes, linearly polarized light experiences an alternating retardation, and the birefringence is averaged to near zero. The inherent linear birefringence, and polarization mode dispersion, can thus be reduced to negligibly low levels [5]. It has proved a major challenge to measure these extremely low residual fiber birefringence levels in the presence of the inevitable externally induced birefringence (due to bending, or mounting of the fiber), which can easily exceed the fiber birefringence. However, by careful control of the fiber handling, it is possible to measure rotations of less than 1° using the polarization modulation technique [6]. The fiber is suspended vertically, attached at the top only, to ensure that no bends or twists are present, and a birefringence modulator placed in series with the fiber. In this way the total throughput polarization retardation can be modulated, greatly simplifying polarizer/analyzer nulling and allowing synchronous detection techniques to be employed [7].

B. Linearly Birefringent Fibers

There are many techniques for producing highly linearly birefringent fibers [8]–[10], but the measurements required are common to all designs.

1. LP_{11} Cutoff Wavelength: Owing to the (possibly) noncircular mode field, the preferred technique is the mandrel wrap method, rather than the mode spot-size measurement. However, owing to the large difference in

the effective indices of the x- and y-polarized modes, it is sometimes possible to resolve two separate modal cutoffs; one corresponding to each of the two modes (see Fig. 1). In this case, the usual interpretation is to take the longer wavelength edge to be the effective cutoff wavelength since, in practice, it is required that both x- and y-polarized light are single moded at the operating wavelength. Note, however, that the difference in cutoff wavelengths for the two modes provides a wavelength window in which truly single-polarization operation of the fiber is possible, since one polarized mode is cutoff while the other is guided [11].

2. Modal Spot Size: In many designs of highly birefringent fibers, the fundamental mode is highly elliptical (ellipticity 2:1), which renders existing techniques for the measurement of spot size, e.g., variable-aperture far field (VAFF), offset splice, etc., unsuitable since they assume an approximately circularly symmetric mode. A technique is therefore required which can take noncircularity into account. The simplest solution is to use a video digitizer operating on the near-field image and to perform a suitable computation on the raw data.

3. Modal Birefringence: In all highly birefringent fibers, the modal birefringence B can be assessed by measurement of the fiber beat length L_p, which is given by:

$$L_p = \frac{2\pi}{\beta_1 - \beta_2} = \frac{\lambda}{B}$$

where β_1 and β_2 are the phase constants of the two polarization modes. A number of techniques, listed as follows, are available for measuring L_p:

a. Observation of side-scattered light: The simplest technique for measuring the beat length is to observe the Raleigh scattered light perpendicular to the fiber axis when both modes are equally excited by circularly polarized light from a laser. The observed scattered light is then periodic, with nulls where the guided light is polarized in the plane of observation. The distance between two minima is then the beat length at that wavelength. For stress-birefringent fibers the birefringence is very nearly wavelength independent [10] and it is sufficient to measure the beat length at a single wavelength (e.g., 633 nm), and extrapolate this to give the birefringence at other wavelengths. For shape-birefringent fibers, however, this does not hold and the birefringence must be measured at the wavelength of operation [12]. (See also Section II-B-3-d below.)

b. Cutback technique: An alternative technique, more suitable for long (> 10 mm) beat length fibers is the cutback technique where circularly polarized light is launched into the fiber and the output polarization state monitored by an analyzer and detector. A short length of fiber is removed from the output end of the fiber and the polarization state remeasured. The beat length is then given by the fiber length required to give a π rotation of the output polarization state. Care must be taken when measuring fibers with very high birefringence to always remove lengths shorter than the expected fiber beat length to avoid any ambiguities.

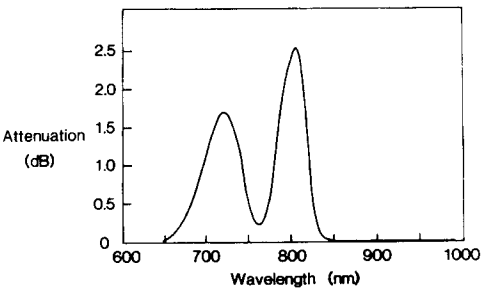

Fig. 1. Spectral separation of the second mode cutoff of the two modes in a linearly birefringent (bow-tie) fiber owing to the large effective difference in effective index of the two modes.

c. Traveling magnet: A small, precision electromagnet with a gap less than the expected beat length is traversed along the fiber and the output polarization state monitored [13]. The magnetic field modulates the local fiber polarization rotation by the Faraday effect and this leads to a periodic variation in the fiber output polarization state as the magnet is moved. Again synchronous detection techniques can be used if the magnetic field is frequency modulated. This technique is difficult to implement in fibers with beat lengths of less than around 1 mm.

d. Wavelength scanning technique: A fiber of accurately known length L (typically a few meters) is placed in the experimental configuration [14] shown in Fig. 2. The polarizer and Wollaston prism are placed at 45° with respect to the principal axes of the fiber. The phase difference ψ between the two orthogonally polarized HE_{11} modes can then be determined from the maximum and minimum output signal intensities I_s and I_b, respectively, since

$$\sin \phi = \pm 2 \frac{\sqrt{I_a I_b}}{I_a + I_b}.$$

Scanning the wavelength λ by a small increment $\Delta\lambda$ induces a phase change $\Delta\psi$ which is expressed by

$$\Delta\psi = \frac{-\Delta\lambda}{\lambda} \frac{2\pi L}{L_p}$$

where L_p is the beat length.

This technique, however, inherently measures the group delay and not only the phase delay between the two polarizer modes [15]. Thus dispersion can seriously affect the accuracy of measuring L_p to between 10 and 20 percent, even in those fibers which have only stress birefringence (bow tie [8], PANDA [9]) and not form birefringence (elliptical core [10]). Nevertheless, the wavelength scanning technique together with an absolute measurement of birefringence at one particular wavelength does yield an accurate measurement of the wavelength dependence of the birefringence.

e. Pressure-induced cross-coupling [16]: Linearly polarized light is launched into the fiber and the output

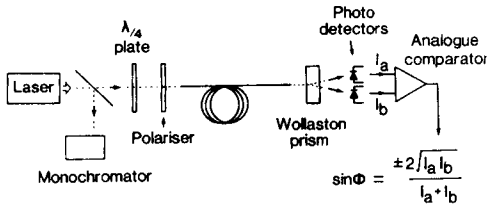

Fig. 2. Experimental configuration for the measurement of birefringence from the phase change induced by scanning the sampling wavelength (after Kikuchi and Okoshi [14]).

monitored through an analyzer. The fiber birefringence is then perturbed by moving a pressure point along its length and counting the nulls in the cross-coupled power. These occur when the polarization vector is parallel or perpendicular to the direction of the force. Thus, if N nulls are counted in length L, then $L_p = 2L/N$.

4. Polarization Cross-Coupling: The polarization-holding ability of a highly birefringent fiber is normally characterized by the so-called h parameter [17] defined as $h = (P_c/P_t)/L$ where P_c and P_t are the cross-coupled and transmitted powers, respectively, and L is the fiber length in meters. The parameter represents the power coupled to the orthogonally polarized mode per unit length. The h parameter is normally measured by launching light from a broad spectrum source ($\sim$5–10 nm), typically an ELED, through a polarizer aligned with one axis of the fiber and monitoring the through and cross-coupled power with an analyzer and detector. Considerable care is required in making this measurement, since small misalignments of either the polarizer or analyzer can cause large errors in the measurement [18], particularly for very small cross-coupling. The quality of the optical components is also of prime importance and strain-free lenses, together with high-quality crystal polarizers, should be used.

It should be noted that the h parameter is strongly dependent on the fiber configuration and packaging and will be worse when the fiber is wound in tight coils or sheathed in badly designed cables. Thus, the h parameter alone may not be, for practical applications, a sensible parameter for describing birefringence in fibers. Theoretical work has shown [19] that the previous interpretation of the h parameter is incorrect, since no account was taken of the role of the fiber birefringence in suppressing bend-induced mode coupling. It can be shown that for significant mode coupling to occur, the correlation length of the applied perturbation must be comparable to the fiber beat length, typically a few millimeters. The currently observed levels of polarization crosstalk cannot, therefore, be due to imperfections within the fiber. They are a consequence of uneven fiber coating and externally applied stresses and bends arising from winding onto a drum. This interpretation is supported by measurements on the effects of different fiber coatings on the h parameter [20]. A possible solution to the measurement of polarization cross-coupling is to define a standard winding which closely resembles the likely environmental stresses the fiber is likely to encounter in a typical application, for instance in a gyroscope coil. If a measure of the resistance of a fiber to polarization cross-coupling is required, the modal birefringence is the best parameter.

The ultimate linear polarization-holding ability of a highly birefringent fiber is limited by Rayleigh scatter, which continuously feeds a small amount of power into the unwanted polarization, and by the fact that the fiber mode is not truly linearly polarized, but exhibits some degree of field curvature. It therefore has both a major and a minor (orthogonally polarized) field component [21]. Polarization crosstalk has been determined as a function of fiber length and it is found that for short lengths of bow-tie fiber, the mode-field curvature limits the transmission of *linearly* polarized light to an extinction ratio of about -40 dB, whereas for a length of 100 km the Rayleigh scattering limit is -30 dB. More recent work with elliptical stress-cladding fibers [18] indicates that a level of -45 dB may be attainable.

The limitations due to the presence of orthogonally polarized minor-field components which are present when measuring the extinction in a short length of fiber with conventional bulk optics [21] may be overcome by the use of a fiber device mode filter to remove the minor-field components. For instance, a short length of conventional monomode fiber can be used to spatially filter (to -70 dB) the minor-field components prior to the polarization analyzer or, alternatively, using a fiber polarizer to replace the bulk optic analyzer in the measurement.

C. Circularly Birefringent Fibers

While many applications require fibers which maintain the state of linear polarization, other sensors require fibers exhibiting a high degree of circular birefringence including, magnetic-field monitoring and electric-current sensors [22], [23]. The main difference in the measurement requirements of the circularly birefringent fiber from those of the linearly birefringent fiber is in determining that the fiber is truly circularly birefringent and not a linearly birefringent fiber with slowly twisted polarization axes. The most certain way of testing for circular birefringence is to vary the wavelength of the linearly polarized launch light, when no polarization ellipticity should result in the output. The simplest technique for measuring the polarization beat length is to use the pressure induced cross-coupling technique described above.

III. Metal/Glass Composite Structures

A. Fiber Polarizer

Several designs of fiber polarizer are available [11], [24]–[26], of which the metal/glass polarizer [25] shown schematically in Fig. 3 provides probably the highest extinction ratio and hence poses the most measurement problems. The fiber contains a hollow D section filled with metal in close proximity to the core which introduces a large differential attenuation between the x- and y-polarized (pseudo-TE and -TM) modes. Spectral attenuation plots for a typical glass/metal polarizer are shown in Fig. 4. An extinction ratio in excess of 37 dB, combined with

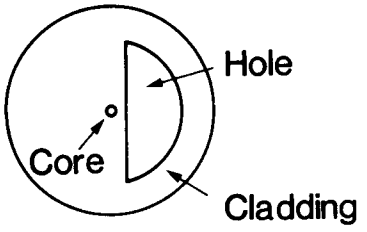

Fig. 3. Schematic of a metal/glass composite fiber polarizer comprising a hollow D section filled with metal close to the fiber core which provides a large differential attenuation between the x (throughput) and y (pseudo -TE and -TM) modes (after Li *et al.* [25]).

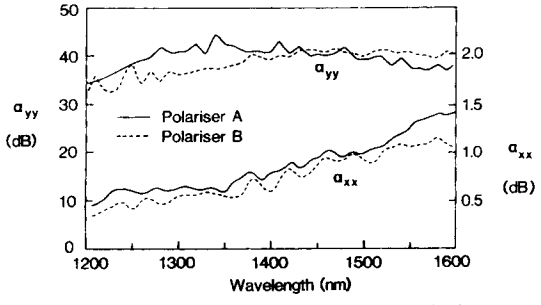

Fig. 4. The spectral dependence of the extinction ratio in a metal/glass composite polarizer (after Li *et al.* [25]).

an insertion loss of less than 1 dB, has been obtained over a wide spectral window (typically 1300 to 1550 nm). This measurement was limited by the equipment used and, to obtain reliable data, care must be taken to reduce the effects of stray light and polarization dependence within the monochromator. Results obtained using a laser source indicate that extinction ratios in excess of 52 dB can be obtained [25].

The performance of a polarizer can only be fully specified by including crosstalk terms in the form of an intensity transfer matrix I between the input and output polarized modes [27]. This matrix has been measured for a coil polarizer with broad-band light from a laser diode, and the results are as follows:

$$I = \begin{pmatrix} T_{xx} & T_{xy} \\ T_{yx} & T_{yy} \end{pmatrix} = T_{xx} \cdot \begin{pmatrix} 1 & R_2 \\ R_1 & R_2R_3 \end{pmatrix} \begin{pmatrix} 2 & -44 \\ -44 & -64 \end{pmatrix} \quad \text{dB}.$$

The choice of measurement method for this intensity transfer matrix requires some care since both attenuation and cross-coupled power for each mode must be determined.

A simple approach involves launching each mode in turn and measuring the output polarization states. This approach requires two cutback reference measurements for each mode launched. Whereas this is acceptable for the measurement of the low-loss mode (T_{xx} = 2 dB) determination of the high loss mode (T_{yy} = 64 dB) is difficult and often needs repeating. A preferable technique requires only one cutback. The transmission ratio for the x-polarized mode, is assessed by the cutback technique. Then, again launching x-polarized light, the output extinction ratio $R_1 = T_{yx}/T_{xx}$ is measured with a prism polarizer. Similarly $R_2 = T_{yy}/T_{xy}$ is obtained while launching y-polarized light. Finally, the power transmission ratio $R_3 = (T_{xy} + T_{yy})/(T_{xx} + T_{yx})$ is measured using the prism polarizer at the fiber input. The measurement of T_{yx} may have been limited by the minor-field components [21], but this is not a limitation for the other terms because the source has the wrong spatial symmetry to launch a mode via its minor-field components.

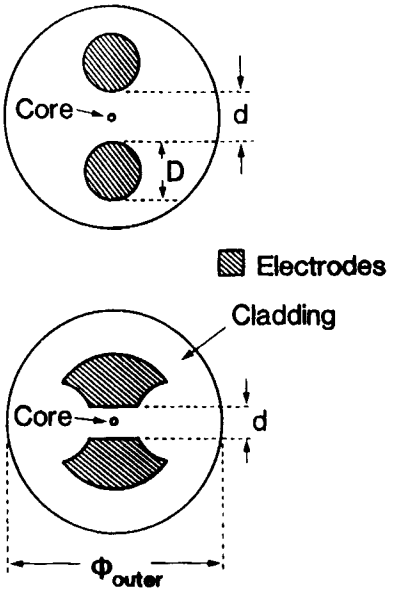

Fig. 5. Kerr modulator fiber showing electrodes on either side of the fiber core, which comprise an indium/gallium mixture (after Li *et al.* [28]).

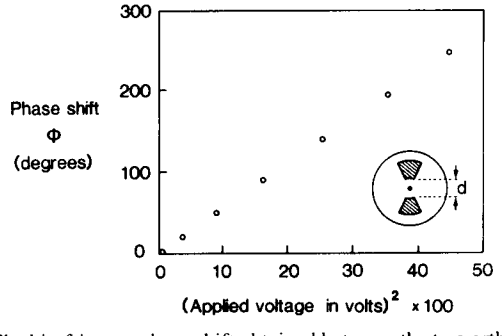

Fig. 6. The birefringent phase shift obtained between the two orthogonally polarized modes of the Kerr fiber. The drive voltage was applied at a frequency of 2 kHz over an interaction length of 30 m (after Li *et al.* [28]).

B. Kerr Modulator Fibers

In addition to the glass/metal fiber polarizers described above, the ability to introduce metal-filled sectors into a fiber leads to the Kerr-effect phase modulator fiber [28] shown schematically in Fig. 5. Here, two electrodes consisting of an indium/gallium mixture are present, one on either side of the fiber core. By applying a voltage to these electrodes, a birefringent phase shift may be obtained between the two orthogonally polarized modes of the fiber, which is proportional to the square of the applied field

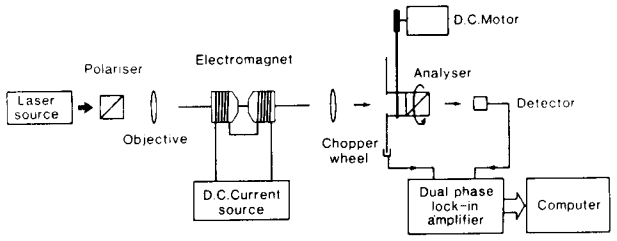

Fig. 7. Experimental configuration for measurement of Verdet constant in an optical fiber. A spun fiber is employed since the fiber under test must have very low internal linear birefringence (after Edwards *et al.* [31]).

(see Fig. 6). Despite the very low electrooptic Kerr effect in silica glass, the long interaction length possible in optical fiber allows the construction of efficient phase modulators. Furthermore, the fibers themselves may be used to measure the nonlinear coefficients of the silica glass—see Section V below.

IV. Measurement of Verdet Constant in Optical Fibers

Fibers fabricated from multicomponent silicate, phosphate, borate, or even chloride glasses may find many applications in areas where the ultralow losses of telecommunications fiber are not required. Such areas include fiber sensors and nonlinear devices where the increased performance obtainable in nonsilicia glasses is more critical than the fiber loss, particularly if only a few meters are required. By using rod-in-tube fabrication techniques, in combination with careful selection of glass properties, it is possible to obtain single-mode fibers with many desirable properties. Indeed, the Verdet constant and nonlinear coefficient $\chi^{(3)}$ can be an order of magnitude higher in soft glasses than in silica [29].

An elegant technique, from an idea by Borelli [30] has been developed by Edwards *et al.* [31] for the measurement of the Verdet constant in nonsilica fibers (Fig. 7). To prevent errors due to interactions between the induced circular and intrinsic linear birefringence, the fiber to be measured must have very low internal linear birefringence and hence a "spun" fiber [4] is used. Plane-polarized light from a laser source is launched into the fiber, which is mounted so as to minimize birefringence introduced by stresses and bends. The rotating-polarizer assembly includes a chopper wheel to provide a reference signal. A dual-phase lock-in amplifier with computer averaging of the output is used to measure the phase difference between the detector and reference signals. A dc magnetic field is applied over a 2 cm length of the fiber with an electromagnet, and the system calibrated by measuring a standard silica fiber (for which the Verdet constant is well known), prior to the nonsilica fiber. Measurements have been made at helium–neon (633 nm) and laser diode (789 nm) wavelengths and the results are given in Table I as the fractional increase in the Verdet constant of Schott F7 glass over silica at both wavelengths. The results indicate a 2.5-fold increase in Verdet constant with a minimum attenuation of 470 dB/km, indicating that this fiber will be useful in current monitor applications if a short length is needed, for instance, in applications requiring a high measurement bandwidth. This technique can be applied to any choice of glass composition, provided that a fiber of low enough birefringence can be fabricated.

TABLE I
Comparison of Properties of Silica and F7 Based Fibers

	Silica fibre	Soft-glass fibre
Core Composition	7 mol.% GeO_2	Schott F7
Cladding Composition	Silica	Schott F2
LP_{11} Cutoff Wavelength	540nm	
Numerical Aperture	0.14	0.13
Cladding Diameter	125μm	160μm
Attenuation 633nm 789nm	17dB/km 4dB/km	770dB/km 490dB/km
Spin Pitch	20mm	8mm
Measured 633nm Relative 789nm Verdet Constant	1 1	2.56 ± 7% 2.59 ± 9%

V. Measurement of Second-Order Nonlinear Coefficients in Optical Fibers

A second-order nonlinearity is necessary for a number of interesting optical effects, such as second harmonic generation (SHG), Pockels effects, and parametric phenomena. Conventionally, second-order nonlinear phenomena are not observable in glasses due to their random structure which results in an inversion symmetry. It has recently been found that the inversion symmetry may be broken [32] and large second-order nonlinear susceptibilities may be induced in special optical fibers by a poling technique [33]. Here defect centers are excited by high-intensity blue light and simultaneously aligned by applying a strong (>100 V/μm) dc electric poling field to the fiber core. When the blue light and the dc field are switched off, the second-order nonlinearity remains permanently frozen into the fiber. The technique is related to the writing of $\chi^{(2)}$ gratings by coherent mixing of a fundamental wave and its second harmonic inside the fiber [32], [34], which, however, produces second-order nonlinearities that are about 100 times smaller than can be induced by fiber poling [35]. We will therefore only discuss measurement techniques related to fiber poling.

A. Second Harmonic Generation (SHG)

The second-order nonlinear coefficient governing SHG, denoted by $\chi^{(2)}$ $(2\omega = \omega + \omega)$, may be measured in two ways. The first method is indirect and is based on a comparison of $\chi^{(2)}$ $(2\omega = \omega + \omega)$ to $\chi^{(3)}$ $(2\omega = \omega + \omega + 0)$, which is the known third-order nonlinear coefficient governing electric-field induced SHG (ESHG) [36]. Since

ESHG is a third-order nonlinear process permitted in glass, it may be observed in unpoled fibers by simply applying a strong dc electric field to the fiber core without the presence of blue light for defect excitation. The process can be viewed as a mixing via $\chi^{(3)}$ of two pump waves at frequency ω with the dc field of zero frequency to give a frequency 2ω.

In the measurement, the SH conversion efficiency η_{ESHG} due to ESHG is determined at a given pump power, prior to poling the fiber. Preferably, the pump is tuned to a wavelength which allows for modal phasematching between the pump and its SH [36] to increase the SH efficiency. (The dc field and optical waves are assumed to be plane parallel to each other.) The fiber is subsequently poled by applying a very high electric field using a fiber of the type shown in Fig. 5 while propagating high-intensity blue light (488 nm) from an argon-ion laser. The SH-conversion efficiency η_{pol} is then remeasured at the same pump power. Provided the excitation signal used in the poling process is incoherent, the second-order nonlinear susceptibility $\chi^{(2)}$ in the poled fiber is given by:

$$\left(\chi^{(2)}_{\text{pol}}\,(2\omega = \omega + \omega)\right)_{111} = \frac{\eta_{\text{pol}}^{1/2}}{\eta_{\text{ESHG}}}\,\frac{O_{\text{ESHG}}}{O_{\text{pol}}}\,\chi^{(2)}_{1111}\,(2\omega = \omega + \omega + 0)E_{\text{dc}}$$

where E_{dc} is the strength of the applied dc electric field for ESHG and O_{ESHG} and O_{pol} are the amplitude overlap integrals for the two nonlinear processes [36]. For example, if the fundamental wave propagates in the LP_{01} mode and the SH in the LP_{02} mode, $O_{\text{ESHG}} \approx O_{\text{pol}} \approx 10$ percent for a V value greater than 2.5 at the pump wavelength. As can be seen, the measurement is a relative one, in which two very similar experiments are compared to observe the increase in $\chi^{(2)}$ due to poling. In this way we avoid having to know exact details of the propagation conditions.

The second technique is based on a more difficult absolute recording of the SH-conversion efficiency at a wavelength at which modal phasematching is achieved. An ESHG measurement is then not necessary. However, in addition to the measurements required in the previous technique, the spatial coherence length L_{coh} between the fundamental and SH wave, i.e., the interaction length, must be known in order to obtain a value for $\chi^{(2)}(2\omega = \omega + \omega)$. Further, the value of the amplitude overlap integral has to be known exactly, whereas, in the first method only a ratio (close to unity) is required. L_{coh} can be obtained by cutback and is typically about 2 cm in a standard fiber. The measurement of such small coherence lengths requires that a length of poled fiber (≈ 10 cm) is spliced onto a length of unpoled fiber. Short lengths of the poled fiber (≈ 5 mm) may then be cut back and the SH-conversion efficiency measured as a function of remaining poled fiber length.

Despite the difficulty of this type of measurement, both techniques have been shown to be in good agreement and a value for $\chi^{(2)}(2\omega = \omega + \omega)$ up to 10 percent of that for KDP has been measured [36]. This remarkably high value indicates that the fiber has assumed crystal-like properties after poling and very high SHG efficiency at low pump powers can be projected.

B. Pockels Effect

The Pockels effect causes a phase shift to occur in an optical wave propagating along the fiber in the presence of a dc field and is also a second-order nonlinear effect not normally found in fibers. The phase shift is linearly proportional to the applied electric field E_{dc} and may thus be used for linear electrooptic modulation. It has again been recently found that a Pockels coefficient r_{11} may be induced in optical fibers simply by applying a strong poling field to the fiber (> 100 V/μm) for several minutes [37] (in this case blue light is not required). As for $\chi^{(2)}(2\omega = \omega + \omega)$ above, r_{11} remains permanently fixed in the fiber after removal of the poling field.

Measurement of the induced Pockels coefficient is somewhat simpler than for SHG. In the following we assume that the fiber is polarization maintaining and that the poling field has been applied along one of the fiber's optical axes, as is the case using the fiber of Fig. 5. The value of r_{11} may then be measured by launching linearly polarized light at 45° to the fiber poling axis and applying a small modulating electric field (modulation frequency $= \omega$) along the poling axis. A compensator is used at the output end to adjust the phase difference (with $E_{\text{dc}} = 0$) of the waves propagating along the two fiber axes to be in quadrature. A polarizer is then inserted at an angle of 45° with respect to the poling axis between the output end of the fiber and a detector. The small modulating field then gives rise to a modulated detector signal of frequency ω with a modulation depth of $2\Delta\Phi$. (Note that the Kerr effect (Section III-B) requires no poling of the fiber since it is a $\chi^{(3)}$-related effect and is easily distinguished from the Pockels effect in that it gives an optical modulation at 2ω as a result of the square-law response to applied field.) The value of the Pockels phase shift $\Delta\Phi$ is given by:

$$\Delta\Phi = \frac{2\pi}{\lambda}\, n^3 r_{11} E_{\text{dc}} L O_p$$

where E_{dc} is the amplitude of the modulated electric field, L is the fiber length, and n is the refractive index at wavelength λ. O_p is the intensity overlap integral for the Pockels effect, which is typically about 80 percent at a wavelength close to that of the cutoff of the second-order mode. Using this measurement technique a Pockels coefficient of 2.1×10^{-15} m/V has been measured in poled fibers [37]. The results for the phase shift $\Delta\Phi$ with applied electric field for both Kerr and Pockels effects are shown in Fig. 8.

VI. Rare-Earth-Doped Fibers

Rare-earth-doped fibers have many applications in fiber technology including both passive [1] (e.g., filters, sensors) and active (e.g., lasers, amplifiers) devices. The un-

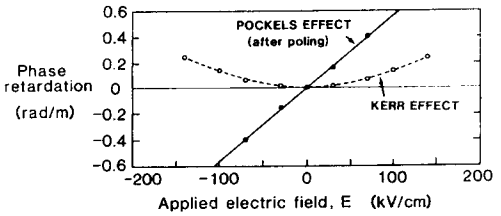

Fig. 8. Comparison of the birefringent phase shift $\Delta\phi$ with applied electric field for both the Kerr effect and the Pockels effect.

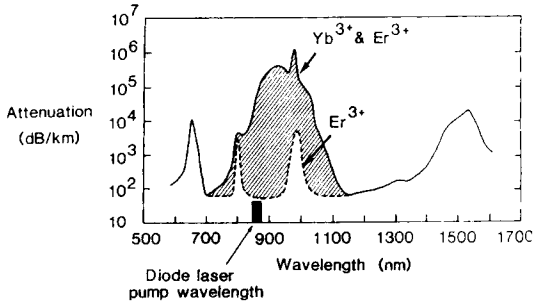

Fig. 9. Spectral attenuation of a fiber containing 550 ppm Er^{3+} and 1.7 percent Yb^{3+} determined by a multiple cutback technique [39] (after Barnes *et al.* [38].)

usual characteristics of these fibers, however, lead to a number of special measurement requirements and solutions.

A. Spectral Attenuation

The measurement of spectral loss of rare-earth-doped fibers requires particular care owing to the intense absorption caused by electron transitions in the rare-earth ions, combined with regions away from the absorptions where the fiber losses approach those of telecommunications fibers. The loss of a fiber containing 550 ppm Er^{3+} and 1.7 percent Yb^{3+} is shown [38] in Fig. 9 where a peak absorption of 1 061 000 dB/km is seen at 980 nm dropping to 60 dB/km at 1150 nm. A multiple cutback method [39] is therefore employed to achieve the dynamic range required, in which several measurements are performed with different fiber lengths over different regions of the spectrum and the results combined. In heavily doped fibers, short fiber lengths (typically <5 cm) are required and the effects of cladding modes may be a problem. To minimize this, a variation on the photon-bucket technique [40] is used in which the fiber under test is spliced between a launch fiber with matched modal spot size and a multimoded receive fiber which captures the attenuated signal.

A partial Dieke diagram of the energy levels in a doped fiber may also be constructed from measurements of spectral absorption at several temperatures [41]. At 77 K, essentially only the true ground state is thermally populated and the wavelengths of the measured absorptions indicate the presence of an energy-level transition. Conversely, at 373 K, thermal population of the ground-state Stark levels gives rise to additional absorption peaks corresponding to transitions from levels above the true ground state. The wavelengths at which excited-state absorption (ESA) is significant can be determined from the Dieke diagram, although the relative intensity of the different bands must be confirmed by the techniques described in Section VI-B below. ESA is a particular problem in glass lasers where the broad absorption bands increase the likelihood of a further transition occurring from an excited state to a higher energy level corresponding to the photon energy of the pump or laser light.

Spectral attenuation measurements are further complicated by the distribution of rare-earth dopant both longitudinally and transversely in the fiber, since both local variations in the dopant concentration along the fiber length and a poor overlap between the radial distribution of dopant and the probe power result in an absorption figure which is unrepresentative of the core material. Measurement of rare-earth axial and radial variations requires specialist techniques which are described below.

1. Longitudinal Variation: The development of distributed sensors [42] or long fiber lasers requires rare-earth-doped fiber having a uniform dopant incorporation over many kilometers. A technique to measure such variations [42] is based on wavelength-tunable OTDR [43]. Here the OTDR signature obtained from a probe pulse, tuned to the edge of an absorption band in order to keep absorption to a minimum, indicates the local concentration of dopant. Loss due to other factors such as core diameter variations and index inhomogeneities are nulled out by sampling from both ends of the fiber, or by using a second probe wavelength in a region where the rare earth does not absorb. Results shown in Fig. 10 indicate that longitudinally inhomogeneous dopant incorporation is rarely a problem [39] in fiber lengths of a few tens of meters.

2. Transverse Variation: It has been shown theoretically [44] and confirmed experimentally [45] that the mode overlap with rare-earth dopant ions significantly affects the performance of active fibers and consequently, measurements are required of the transverse dopant distribution within a fiber or preform.

A qualitative measurement of dopant distribution can be obtained by scanning the output from a laser, tuned to an absorption band of the ion to be measured, across a polished preform sample and measure the variation in either the laser absorption or the fluorescence power. An alternative technique which gives a quantitative measure of the dopant concentration is wavelength dispersive electron probe microanalysis (EPMA) [45], although care is required to ensure correct calibration if accurate results are required. For both measurements, the dopant distribution is determined from preform samples or large core fibers [46] owing to the limited resolution (typically 2 μm) of the measurement systems (see Fig. 11). Knowledge of the dopant distribution may then be used to modify the fabrication process and hence optimize the radial dopant profile for device applications [45].

B. Excited-State Absorption (ESA)

In any rare-earth-doped laser system, the effect of ESA is to reduce the laser efficiency and it may even prevent

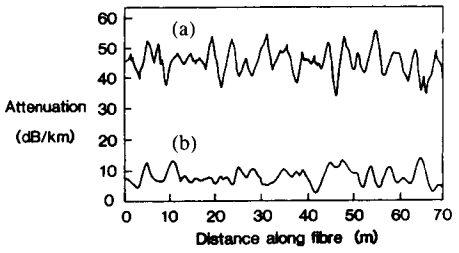

Fig. 10. Local attenuation of fibers showing the average uniformity over length obtained using an OTDR technique (after Poole *et al.* [39]). (*a*) Nd^{3+}-doped fiber, and (*b*) undoped fiber.

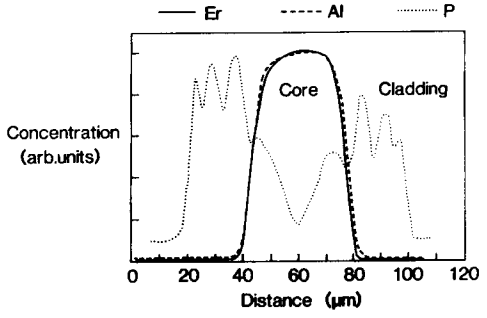

Fig. 11. A typical elemental distribution of Er^{3+}, Al, and P across an Er^{3+}-doped Al_2O_3-P_2O_5-SiO_2 fiber core (after Ainslie *et al.* [46]).

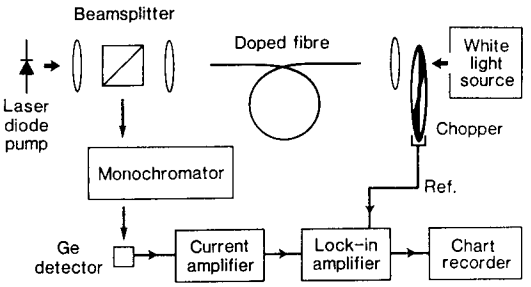

Fig. 12. Experimental configuration for the measurement of signal or pump ESA in a doped optical fiber (after Morkel *et al.* [41] and Laming *et al.* [50]).

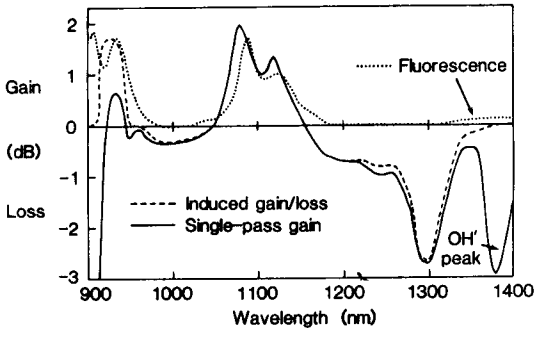

Fig. 13. Spectral characteristics of signal Gain/ESA and fluorescence for a Nd^{3+}-GeO_2/SiO_2 fiber. The dashed curve shows the ratio of pumped and unpumped fiber output and indicates the regions over which stimulated emission and excited-state absorption occur. Including the unpumped loss of the fiber gives the solid curve which therefore indicates the single pass gain or loss of the fiber (after Morkel *et al.* [41]).

lasing at some wavelengths, even though there appears to be considerable fluorescence present [41]. As noted previously, there are two types of ESA: signal ESA in which there is an absorption from the metastable level to a higher level whose wavelength corresponds to that of the emission wavelength, and pump ESA which depletes the metastable level by absorption of pump photons in a transition from the metastable to a higher energy level. A knowledge of the ESA is therefore required to determine suitable operation and pump wavelengths for these devices. It may also be useful to modify the core glass composition, as it is known that this can alter the absorption cross section of the dopant ion at a given wavelength and may also shift the ESA band(s).

1. Signal ESA: To measure signal ESA, the configuration of Fig. 12 is used [41]. Here, the fiber is pumped through a beam splitter or dichroic coupler with a semiconductor laser. The induced gain and excited-state absorption under this pumping condition is measured using a spectrophotometer consisting of a counter-propagating white-light signal, a monochromator, and a suitable detector. Typical results for a Nd^{3+}-doped fiber with a GeO_2/SiO_2 core are shown in Fig. 13. Here, the dashed curve shows the ratio of pumped and unpumped fiber output and indicates the regions over which stimulated emission and excited-state absorption take place. Including the unpumped loss of the fiber gives the solid curve which therefore indicates the single pass gain or loss of the fiber as a function of wavelength. The dotted curve shows the fluorescence output of the fiber under the same pumping conditions for comparison with the gain curve. It should be noted that the fluorescence has not been corrected for material reabsorption and excited-state absorption. The effect of this will be to partially reabsorb the fluorescence at certain wavvelengths. However, the wavelengths where fluorescence is observed indicates spectral regions in which a finite stimulated-emission cross section exists (i.e., the potential for gain). It is also interesting to note that the observed excited-state absorption extends into the fluorescence regions at 1160, 1050, and 980 nm and thus limits the potential wavelength tuning ranges of Nd^{3+} lasers operating on the $^4F_{3/2} - {}^4I_{11/2}$, $^4I_{9/2}$ transitions. The peak gain is seen at 1088 and 938 nm which is consistent with the lasing properties of the fiber at these wavelengths [47], [48].

The importance of ESA measurements is clearly seen by considering the region around 1300 nm where apparently a loss is induced by pumping the fiber, indicating that an excited-state absorption exists. Although the $^4F_{3/2} - {}^4I_{13/2}$ fluorescence peaks at around 1370 nm, no gain is found at this wavelength implying that any stimulated emission is being counteracted by the ESA centered on 1300 nm.

2. Pump ESA: Pump ESA in Er^{3+}-doped fibers has been investigated [49], [50] using similar apparatus to that shown in Fig. 12. Chopped white light from a tungsten lamp was launched into one end of a short length of doped fiber and the output analyzed with a monochromator (FWHM −2 nm), Si-p-i-n photodiode, lock-in ampli-

fier, and computer. Counterpropagating pump light (from either a color-center laser operating at a wavelength of 1.549 μm or a polarized dye laser at 665 nm) is coupled in via a polarizing beam splitter. The fiber throughput was measured both pumped and unpumped to obtain the ESA spectrum, following which the fiber was cut back and remeasured to obtain a value for the unpumped loss, i.e., the ground-state absorption (GSA).

A typical result is shown in Fig. 14 for an Er^{3+}-doped fiber having an Al_2O_3/SiO_2 core composition. The spectrum is plotted from 750–1050 nm, which includes the important diode-pumpable $^4I_{15/2}$–$^4I_{9/2}$ transition occurring at about 807 nm. At this wavelength it can be seen that the ESA extends across the entire ground-state absorption, indicating that much of the pump light will be dissipated inefficiently as heat. Conversely, the $^4I_{15/2}$–$^4I_{11/2}$ transition, centered on 980 nm, was also investigated and, as can be seen, no ESA whatsoever was observed, which agrees with the expected result from a study of energy-level diagrams. This result indicates the importance of ESA measurements, since they permit the identification of an ideal pump wavelength for maximum efficiency.

A figure of merit indicating the significance of the pump ESA at any given wavelength is the ratio $\sigma_{ESA}/\sigma_{GND}$ where σ_{ESA} and σ_{GND} are the excited- and ground-state absorption cross sections, respectively. Ideally, for a prospective pump absorption band this ratio should be zero, but the lower the ratio, the lower the ESA. The ratio of absorption cross sections for the Er^{3+} in a number of host glasses is tabulated for all available pump wavelengths in Table II [50].

C. Fluorescence Measurements in Rare-Earth-Doped Fibers

Several parameters must be measured for the determination of fluorescence characteristics. Of particular importance are the spectral output and decay time but, additionally, excited-state and broadening effects must be quantified.

1. Spectral Characteristics: A typical fluorescence measurement configuration [39] is shown in Fig. 15. Phase-sensitive detection increases the signal-to-noise ratio of the weak output which is of the order of 50 fW over a 5-nm bandwidth for a 15-mW pump. Owing to the long interaction lengths in fibers, reabsorption of emission can seriously affect the output spectrum [51], particularly in three level systems in which there is a strong absorption band at the fluorescence wavelength. Two methods are commonly employed to overcome this effect. Fluorescence is measured from a length of fiber which is substantially shorter than the absorption length or orthogonally to the launched plane in a fiber or polished sample of preform [52]. In each case reabsorption of the fluorescence is avoided.

In a three level system, such as Er^{3+}, competition between the ground-state absorption and excited level fluorescence causes an evolution of the net signal-gain spectrum along the fiber. The effect is seen by changes in the amplified spontaneous emission (ASE) spectrum under different pump conditions (different population inversion conditions). Distortion of the emission spectrum is avoided by measurement of side-scattered signal as described above.

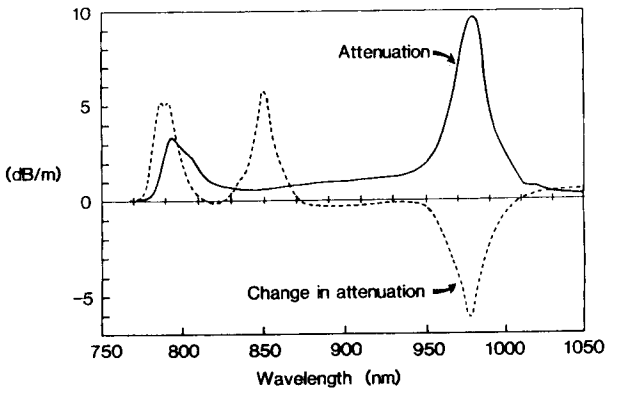

Fig. 14. Spectral characteristics of pump ESA in an Er^{3+}-doped fiber with an Al_2O_3–SiO_2 core (after Laming *et al.* [50]).

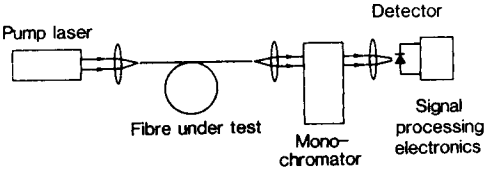

Fig. 15. Experimental configuration for measurement of fluorescence in a rare-earth ion doped optical fiber (after Poole *et al.* [39]). Signal reabsorption effects are avoided by measurement of end face fluorescence. Signal processing electronic consists of a phase-sensitive detector for fluorescence spectra or a computer-controlled digital averager for fluorescence lifetime measurements.

TABLE II
RATIO OF EXCITED-STATE AND GROUND-STATE ABSORPTION CROSS SECTIONS $\sigma_{ESA}/\sigma_{GND}$ AS A FUNCTION OF WAVELENGTH

Fibre Type Wavelength (nm)	GeO_2	GeO_2/B_2O_3	GeO_2/P_2O_5	Al_2O_3
488	2.9		1.86	1.74
514.5	0.95		0.55	0.5
655	0.28	0.25	0.13	0.14
810	2.0	2.0	1.0	1.0
980				0

Further, it has been found that fluorescence spectra depend on the source characteristics for Nd^{3+}. The effect of both pump power and pump wavelength on emission spectra has been measured [41]. No special modifications to the measurement configuration already described are necessary.

2. Time-Dependent Characteristics: Fluorescence decay-time characteristics of rare-earth-doped fibers are determined using the equipment shown in Fig. 15 where the signal-processing electronics comprises a computer-con-

trolled digital averager triggered by the laser pump. The exponential decay in output intensity with time after pulsed excitation is measured and curve fitted to determine the increase in the value of the $1/e$ fluorescence decay time. Owing to the statistical distribution of the dopant ions in the glass host, the decay time constant tends to increase in the tail of the fluorescence pulse. Moreover, it has been shown in heavily Nd^{3+}-doped fibers that the radiative decay time can be resolved into a fast and a slow component [53]. The fast component is due to concentration quenching in clustered ions and reduces lasing efficiency. The effect can be reduced in fibers by appropriate choice of host material in which the dopant ions are more readily soluble [53].

Fluorescence decay time measurements can be extended to the measurement of energy transfer efficiency [54] in codoped fibers [55]. The technique has been applied to Er^{3+}–Yb^{3+} codoped fibers in which laser action of the Er^{3+} system is achieved by pumping indirectly via the Yb^{3+} ions which can be excited by a readily available diode pump source [56]–[58] at 810–830 nm. The efficiency of energy transfer is determined from the fractional change in fluorescence decay time of the Yb^{3+} fluorescence in a codoped fiber compared with the Yb^{3+} emission in an equivalent, singly doped fiber and indicates the potential for laser action [35], [59].

VII. Active Fiber Devices

A. Spectral Properties

In common with other laser sources, the spectral properties of a fiber laser are determined by the characteristics of the gain medium and laser resonator, such as spontaneous emission bandwidth, fiber length, and mirror reflectivities. Additional factors include etalon and couple cavity effects and the reflection bandwidth of frequency-selective gratings.

The spectral width of a fiber laser output ranges from in excess of 10 nm (3 THz) for a conventional neodymium-doped fiber CW laser configuration, to around 1 MHz for a single longitudinal-mode configuration employing a fiber grating [60]. This necessitates the use of very different techniques to determine the spectra at these two extremes of operation. In addition, fiber lasers can be constructed with lengths from a few centimeters to over a kilometer, depending on the dopant concentration. These lengths give Fabry–Perot longitudinal mode spacings of between 5 GHz and 150 kHz.

Conventional grating monochromators are used to provide spectra down to 0.01-nm resolution, which is insufficient to resolve the Fabry–Perot modes of the laser output for all but the shortest fiber laser. However RF spectral analysis using fast detection apparatus ($>=$ 100 MHz) reveals intermodal beats at the cavity round-trip frequency, indicating the presence of the Fabry–Perot modes. Additional spectral information can be obtained by using a Fabry–Perot scanning interferometer, with resolution to the order of 10 MHz.

To resolve the spectrum of a single longitudinal-mode fiber laser the delayed self-heterodyne technique first proposed by Okoshi *et al.* [61] is required. This method is based on the standard heterodyne technique, but overcomes the problem of obtaining a stable narrow-line oscillator by using a time-delayed component of the signal from the laser under test to provide local oscillator power, as shown in Fig. 16. The laser output is split into two paths, one of which passes either through a frequency shifter (e.g., acoustooptic or electrooptic modulator) and the other through a delay line consisting of a single-mode optical fiber. Measurement resolution is determined by the fiber length, which must be chosen so that the signals from the two paths can be considered statistically independent. The two signals are mixed and the combined result is measured on an RF spectrum analyzer to estimate the laser linewidth, the actual linewidth being half the width of the observed spectrum. It can be shown [62] that the narrowest measurable spectral width Δf_{FWHM}, is given by:

$$\Delta f_{\mathrm{FWHM}} = \frac{6 \times 10^8}{\Pi . l}$$

where l is the length of the fiber delay line.

Using 1 km of fiber, submegahertz linewidths can easily be characterized using this technique. Fiber laser phase-noise-induced linewidths measured in this manner are in reasonable agreement with the Schawlow–Townes quantum limit [63].

B. Cavity Losses

A fiber laser resonator consists, in general, of a length of rare-earth-doped fiber, a mirror butted to each cleaved end, and various intracavity components, such as acoustooptic Q-switches and 4-port couplers. An indication of the excess loss in the resonator (i.e., excluding output coupling) is desirable in order to predict the optimum value of the output coupling. Two techniques have been developed to measure the cavity loss, one based on a passive cavity ring-down technique [64] and the other using measurements of relaxation times in a lasing cavity [65]. The experimental configuration for the former is shown in Fig. 17. Short (150 ns) pulses from a Q-switched Nd:YAG laser operating at 1.064 μm are injected into the passive (i.e., umpumped) fiber laser resonator which contains Nd^{3+}-doped fiber. The cavity round-trip path length was chosen to be long (191 m) compared to the Q-switched pulse length to prevent any pulse overlap effects within the fiber resonator. Each pulse from the Nd:YAG laser injected into the cavity shuttles back and forth giving rise to an exponentially decaying train of pulses from the output mirror. The spacing of the pulses gives the cavity round-trip delay time and the decay of the pulse envelope gives the round-trip feedback. To emphasize the effect of intracavity losses, the two mirrors were chosen to have maximum reflectivity ($>$99.8 percent) at 1.064 μm. Although this gives a good measure of the excess losses, very little light emerges from the output mir-

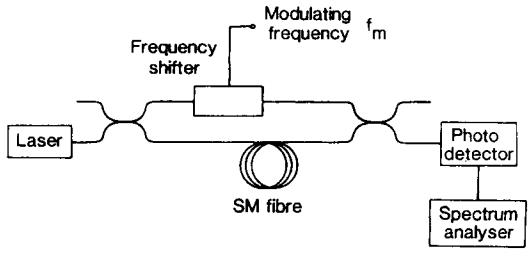

Fig. 16. Experimental setup for the measurement of the laser spectrum based on the self-heterodyne measurement. The fiber laser output is split into two paths, through a frequency shifter or an optical fiber delay line and the linewidth is estimated from the result of the combined signals (after Cowle [62]).

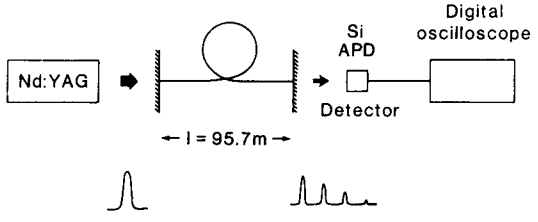

Fig. 17. Experimental passive-cavity configuration for the measurement of cavity losses by the cavity ring-down technique (after Morkel *et al.* [64]).

ror and digital signal averaging is needed to recover the signal.

After an integer number N of cavity round trips, the intensity feedback can be written as

$$\log_{10}(\text{feedback}) = N\left(-2\alpha L/10^4 + \log_{10}\left(R_1R_2\,(1-k)\right)\right)$$

where

α	fiber loss in decibels/kilometer,
N	number of cavity round trips,
L	fiber length,
R_1, R_2	mirror reflectivities,
k	loss incurred at two mirror butts.

A typical result is shown in Fig. 18, in which $\log_{10}$ (feedback) is plotted as a function of round-trip number. The slope of the line gives the round-trip loss and knowing the fiber loss to be (4 ± 0.5) dB/km, we can deduce that in this case $k < 4$ percent. Thus each individual butt loss represents a loss of only 0.1 dB. Knowing the intracavity loss it is possible to determine the optimum output coupling for a given cavity from well-known expressions [63] and thus it permits *in situ* optimization of fiber laser performance.

A similar technique, using relaxation oscillations in a fiber laser cavity, has also been described [64]. Here, relaxation oscillations were induced in a fiber laser by modulating the output of the pump laser (in this case a semiconductor diode) and plotting the relaxation oscillation frequency as a function of launched power. From this, the cavity decay time, and hence the cavity loss can be obtained.

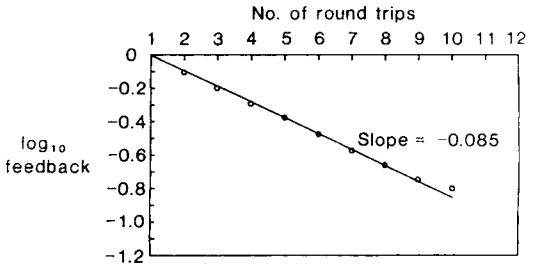

Fig. 18. A typical result obtained from the cavity ring-down technique where the slope of the relationship between $\log_{10}$ (feedback) and number of cavity round trips gives the round-trip loss (after Morkel *et al.* [64]).

C. Noise Measurements in Fiber Amplifiers

Amplifiers which are based on Er^{3+}-doped amplifiers are expected to have a major impact on telecommunications systems operating in the third window at 1.55 μm. Noise measurements are perhaps the most pressing requirement, since, although all optical amplifiers have been shown both experimentally [66]–[71] and confirmed theoretically [72], [73], to operate near the quantum noise limit, in practice, practical considerations such as stray reflections, extraneous noise sources (pump noise, interchannel crosstalk) and coherent backscatter will play a part.

The output from an optical fiber amplifier is a combination of amplified signal and broad-spectrum amplified spontaneous emission (ASE). If the input signal is coherent, its noise contribution is the usual shot noise associated with the amplified signal level. There is also shot noise associated with the level of ASE. Additional noise terms are introduced by the mixing on the detector of the amplified signal and the spectral components of the ASE to give signal–spontaneous beat noise and spontaneous–spontaneous beat noise [74].

The power spectral density of the signal–spontaneous beat noise is independent of the optical bandwidth, whereas spontaneous–spontaneous beat noise is a direct function of optical bandwidth. Thus reducing the optical bandwidth reduces the spontaneous–spontaneous beat noise contribution and at low power levels where this noise dominates, optical filtering can be an advantage [67], [74].

The amplifier noise performance can be characterized by measuring the amplifier output signal-to-noise ratio (SNR) or the bit error rate (BER) for a range of input signal levels and amplifier gains. In this way detail of the intrinsic noise mechanisms in the amplifier can be obtained. A typical experimental set [66] for SNR measurements is shown in Fig. 19. Here the ends of the erbium-doped fiber are terminated so as to eliminate reflections into the amplifier. Light of constant power from a pump laser and variable signal power from a DFB semiconductor laser are coupled into the amplifier either at the same end (copropagating geometry) or at opposite ends (counterpropagating) as shown. The narrow-linewidth DFB laser wavelength is temperature tuned to the peak of the gain curve for the erbium-doped fiber.

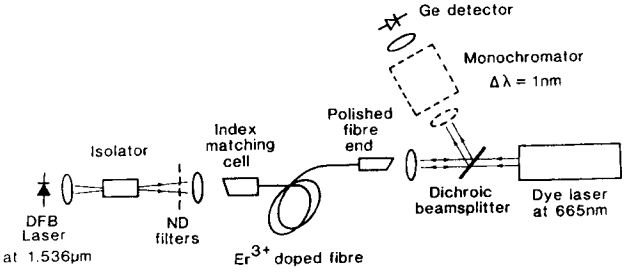

Fig. 19. Configuration for the measurement of SNR in an optical fiber amplifier (after Laming *et al.* [66]). Receiver losses and those between the fiber and receiver can mask the true noise characteristics and must be minimized. In addition a large dynamic range is required to cope with the range of amplified signal levels.

The amplified signal is measured using a low noise receiver and analyzed with an RF spectrum analyzer. The receiver must have a large dynamic range (-40 dB) to cope with the range of amplified signal levels and have a lower noise than both the ASE and amplified signal shot noise. Additionally, any loss between the amplifier output and receiver must be minimized as this can mask the true amplifier noise characteristics. This approach was adopted by Laming *et al.* [66] and has demonstrated that near quantum limited amplifier performance is possible when care is taken to ensure a sufficiently high pump intensity at the amplifier input [72], [73]. This is satisfied with the copropagating geometry. From these results it is concluded that, as a preamplifier, the predicted maximum sensitivity for a 10^{-9} BER in a 1-GHz bandwidth is -45 dBm (peak to peak) with optical filtering and -41.5 dBm (peak to peak) unfiltered.

Alternatively, systems type measurements of BER can provide information as to amplifier performance. A similar experimental geometry to that of Fig. 19 is employed but the DFB is direct modulated or subsequently modulated with a $LiNbO_3$ switch to provide the digital source. The received signal is then analyzed with conventional BER test equipment to determine the BER and thus SNR. These types of measurements have been performed and the erbium fiber amplifier performance [68], [71] has been tested up to 2 Gbit/s. However, large losses between the amplifier and receiver and also imperfect electronics have masked the true amplifier noise in most cases. But, the work of Pettitt *et al.* [70] has confirmed that erbium-doped optical fiber amplifers can be operated near the quantum limit. Further, there is an intrinsic problem with the measurement of amplifier noise with BER systems for large signal input intensities (> -30 dBm) owing to the excellent noise performance of these amplifiers. However, BER characteristics can be predicted from measurements of SNR in this input signal region.

VIII. Conclusions

The special waveguiding properties of fibers designed for sensor applications have created particular measurement problems, however much effort has been directed to overcoming these. Birefringence, both intrinsically very low or high, can now be measured by several methods and, although the precise method must be chosen with care, a complete characterization is readily obtained. The determination of nonlinear coefficients is, in general, more difficult and comparative measurements are frequently required. Verdet constant measurements are made in this manner, with the characteristics of the fiber under test being compared with the well-known properties of silica. Nevertheless, absolute measurements of nonlinear coefficients are possible.

Characterization of rare-earth ion doped fibers is hindered by the intense absorption bands due to the dopant ions but, by careful choice of fiber length and experimental configuration, absorption, fluorescence, and backscatter measurements can be obtained from modified conventional systems. In addition, standard materials methods have been adopted for the analysis of the dopant ions and glass components. Techniques have also been developed from laser technology for the full determination of active fiber devices, but characterization of the amplifier BER performance has been more difficult to achieve since conventional measurements systems are not themselves sufficiently low noise, however, predictions can be made from SNR results.

To conclude, measurement techniques have been developed to analyze the wide range of fibers now available and although, in many cases, data are difficult to obtain, the literature confirms that these novel fibers can be characterized.

Acknowledgment

The authors would like to thank Pirelli General plc for providing a Readership (D.N.P.), a Senior Research Fellowship (S.B.P.), and a Research Fellowship (R.I.L.). A Research Fellowship (P.R.M.) was funded by British Aerospace and a student scholarship (G.J.C.) was provided by the Association of Commonwealth Universities.

References

[1] D. N. Payne, "Fibers for sensors," in *Proc. OFS* (Stuttgart, W. Germany), 1984, pp. 353-360.
[2] G. A. Pavlath, "Fiber-optic gyro development at Litton," *Proc. SPIE, Int. Soc. Opt. Eng. (USA)*, vol. 219, pp. 24-27, 1987.
[3] D. N. Payne, S. B. Poole, M. P. Varnham, and R. D. Birch, "Characterization of speciality fibers and components," in *Tech. Dig. Symp. Opt. Fiber Meas.* (Boulder, CO), 1986, pp. 107-113.
[4] A. J. Barlow, D. N. Payne, M. R. Hadley, and R. J. Mansfield, "Production of single-mode fibers with negligible intrinsic birefringence and polarization mode dispersion," *Electron. Lett.*, vol. 17, pp. 725-726, 1981.
[5] D. N. Payne, A. J. Barlow, and J. J. Ramskov-Hansen, "Development of low- and high-birefringence optical fibers," *IEEE J. Quan-*

tum Electron., vol. QE-18, pp. 477-487, 1982.
[6] A. J. Barlow and D. N. Payne, "Measurements of fiber polarization properties using a photoelastic modulator," in *Tech. Dig. Symp. Opt. Fiber Meas.* (Boulder, CO), 1982, pp. 101-104.
[7] A. J. Barlow, "Optical fiber birefringence measurement using a photoelastic modulator," in *Tech. Dig. Symp. Opt. Fiber Meas.* (Boulder, CO), 1983.
[8] R. D. Birch, D. N. Payne, and M. P. Varnham, "Fabrication of polarization-maintaining fibers using gas-phase etching," *Electron. Lett.*, vol. 18, pp. 1036-1038, 1982.
[9] Y. Sasaki, K. Okamoto, T. Hosaka, and N. Shibata, "Polarization-maintaining and absorption-reducing fibers," in *Proc. OFC* (Phoenix, AZ), Jan. 1982, pap. ThCC6.
[10] R. B. Dyott, J. R. Cozens, and D. G. Morris, "Preservation of polarisation in optical fibre waveguides with elliptical cores," *Electron. Lett.*, vol. 15, pp. 380-382, 1979.
[11] M. P. Varnham, D. N. Payne, R. D. Birch, and E. J. Tarbox, "Single-polarisation operation of highly birefringent bow-tie optical fibres," *Electron. Lett.*, vol. 19, pp. 246-247, 1983.
[12] S. C. Rashleigh, "Origins of polarization in single-mode fibers," *J. Lightwave Technol.*, vol. LT-1, pp. 312-331, 1983.
[13] A. Simon and R. Ulrich, "Evolution of polarization along a single-mode fiber," *Appl. Phys. Lett.*, vol. 31, pp. 517-520, 1977.
[14] K. Kikuchi and T. Okoshi, "Wavelength-sweeping technique for measuring the beat length of linearly birefringent optical fibers," *Opt. Lett.*, vol. 8, pp. 122-123, 1983.
[15] S. C. Rashleigh, "Measurement of fiber birefringence by wavelength scanning; Effect of dispersion," *Opt. Lett.*, vol. 8, pp. 336-339, 1983.
[16] N. Chinone and R. Ulrich, "Elastooptic polarization measurement in optical fiber," *Opt. Lett.*, vol. 6, pp. 16-18, 1981.
[17] D. Marcuse, "Coupled-mode theory for anisotropic waveguides," *Bell Syst. Tech. J.*, vol. 54, pp. 985-995, 1975.
[18] F. M. Sears, "Cross-polarization limits in polarization-maintaining fibers and measurements," in *Proc. OFC'88*, pap. WA4, pp. 343-344.
[19] F. P. Payne, D. N. Payne, and M. P. Varnham, "Crosstalk in polarization-maintaining fibers," in *Proc. ECOC* (Barcelona, Spain), Sept. 1987, pp. 239-242.
[20] Y. Kikuchi, K. Himeno, N. Kawakami, F. Suzuki, and O. Fukuda, "Ultralow crosstalk polarization-maintaining fiber in a short length operation," in *Proc. OFC 86* (Atlanta, GA), Feb. 1986, p. 36.
[21] M. P. Varnham, D. N. Payne, and J. D. Love, "Fundamental limits to the transmission of linearly polarized light by birefringent optical fibers," *Electron. Lett.*, vol. 20, pp. 55-56, 1984.
[22] L. Li, J. R. Qian, and D. N. Payne, "Current sensors using highly birefringent bow-tie fibers," *Electron. Lett.*, vol. 22, pp. 129-130, 1986.
[23] R. D. Birch, "Fabrication and characterization of circularly birefringent helical fibres," *Electron. Lett.*, vol. 23, pp. 50-52, 1987.
[24] T. Okoshi and K. Oyamoda, "Single-polarization single-mode optical fibre with refractive-index pits on both sides of the core," *Electron. Lett.*, vol. 16, pp. 712-713, 1980.
[25] L. Li, G. Wylangowski, D. N. Payne, and R. D. Birch, "Broad-band metal/glass single-mode fiber polarizers," *Electron. Lett.*, vol. 22, pp. 1020-1022, 1986.
[26] R. B. Dyott, J. Bello, and V. A. Handerek, "Indium-coated D-shaped-fiber polarizer," *Opt. Lett.*, vol. 12, pp. 287-289, 1987.
[27] M. P. Varnham, D. N. Payne, A. J. Barlow, and E. J. Tarbox, "Coiled-birefringent fiber polarizers," *Opt. Lett.*, vol. 9, pp. 306-308, 1984.
[28] L. Li, R. D. Birch, and D. N. Payne, "An all fiber electrooptic Kerr modulator," in *Proc. IEE Colloq. Advanced Fiber Waveguide Devices* (London, England), May 1986.
[29] R. Adair, L. L. Chase, and S. A. Payne, "Nonlinear refractive measurements of glasses using three wave frequency mixing," *J. Opt. Soc. Amer.*, Ser. B, vol. 4, pp. 875-881, 1987.
[30] N. F. Borelli, "Faraday rotation in glasses," *J. Chemical Phys.*, vol. 41, pp. 3289-3293, 1964.
[31] H. O. Edwards, K. P. Jedrzejewski, R. I. Laming, and D. N. Payne, "Optimal design of optical fibers for electric current measurement," *Opt Lett.*, submitted for publication.
[32] U. Österberg and W. Margulis, "Efficient second harmonic generation in an optical fiber," presented at the IQEC 86, San Francisco, CA, pap. WBB2.
[33] M. V. Bergot, M. C. Farries, M. E. Fermann, L. Li, L. J. Poyntz-Wright, P. St. J. Russell, and A. Smithson, "Generation of permanent optically induced second-order nonlinearities in optical fibers by poling," *Opt. Lett.*, vol. 13, pp. 592-594, 1988.
[34] R. H. Stolen and H. W. K. Tom, "Self-organized phase-matched harmonic generation in optical fibers," *Opt. Lett.*, vol. 12, pp. 585-587, 1987.
[35] M. E. Fermann, "Characterisation techniques for special optical fibres," Ph.D. dissertation, Univ. of Southampton, Hants., England, 1988.
[36] M. E. Fermann, L. Li, M. C. Farries, and D. N. Payne, "Frequency doubling by modal phase matching in poled optical fibers," *Electron. Lett.*, vol. 24, pp. 894-895, 1988.
[37] L. Li and D. N. Payne, "Permanently induced linear electrooptic effect in silica optical fibers," to be presented at IGWO 89, Houston, TX, 1989.
[38] W. L. Barnes, D. J. Taylor, M. E. Fermann, J. E. Townsend, L. Reekie, and D. N. Payne, "A diode-laser-pumped Er^{3+}/Yb^{3+}-doped fiber laser operating at 1.57 μm," to be presented at OFC 89, Houston, TX, 1989.
[39] S. B. Poole, D. N. Payne, R. J. Mears, M. E. Fermann, and R. I. Laming, "Fabrication and characterization of low-loss optical fibers containing rare-earth ions," *J. Lightwave Technol.*, vol. 4, no. 7, pp. 870-876, 1986.
[40] W. C. Young, "Stress-induced increase in interference effects at fiber joints and a method to eliminate interference effects in optical fiber measurements," in *Tech. Dig. Symp. Opt. Fiber Meas.* (Boulder, CO), 1986.
[41] P. Morkel, M. C. Farries, and S. B. Poole, "Spectral variation of excited-state absorption in neodymium-doped fiber lasers," *Opt. Commun.*, vol. 67, pp. 349-352, 1988.
[42] M. C. Farries, M. E. Fermann, R. I. Laming, S. B. Poole, and D. N. Payne, "Distributed temperature sensor using Nd^{3+}-doped optical fiber," *Electron. Lett.*, vol. 22, no. 8, pp. 418-419, 1986.
[43] A. J. Conduit, A. H. Hartog, and D. N. Payne, "Spectral variation and length dependence losses in optical fibres investigated by a two channel backscatter technique," *Electron. Lett.*, vol. 16, no. 3, pp. 77-78, 1980.
[44] M. J. F. Digonnet and C. J. Gaeta, "Theoretical analysis of optical fiber laser amplifiers and oscillators," *Appl. Opt.*, vol. 24, no. 3, pp. 333-342, 1985.
[45] B. J. Ainslie, J. R. Armitage, S. P. Craig, and B. Wakefield, "Fabrication and optimization of the erbium distribution in silica based optical fibers," in *Proc. ECOC* (Brighton, England), 1988, pp. 62-65.
[46] B. J. Ainslie, S. P. Craig, S. T. Davey, and B. Wakefield, "The fabrication, assessment, and optical properties of high concentrations of Nd^{3+} and Er^{3+}-doped silica based fibers," *Mater. Lett.*, vol. 6, pp. 139-144, 1988.
[47] S. B. Poole, L. Reekie, R. J. Mears, and D. N. Payne, "Neodymium-doped silica single-mode fiber lasers," *Electron. Lett.*, vol. 21, pp. 738-740, 1985.
[48] I. P. Alcock, A. I. Ferguson, D. C. Hanna, and A. C. Tropper, "Continuous-wave operation of a monomode neodymium-doped fiber laser at 0.9 μm on the $^4F_{3/2}$-$^4F_{9/2}$ transition," *Opt. Commun.*, vol. 58, pp. 405-408, 1986.
[49] J. R. Armitage, C. G. Atkins, R. Wyatt, B. Ainslie, and S. P. Craig, "Spectroscopic studies of Er^{3+}-doped single-mode silica fiber," in *Proc. OSA* (Williamsburg, VA), 1987, pap. WD3.
[50] R. I. Laming, S. B. Poole, and E. J. Tarbox, "Excited-state absorption in erbium-doped fibers," *Opt. Lett.*, to be published.
[51] Y. Kimura and M. Nakazawa, "Lasing characteristic of Er^{3+}-doped silica fibers from 1553 nm up to 1603 nm," *J. Appl. Phys.*, vol. 64, no. 2, pp. 516-520, 1988.
[52] B. J. Ainslie, S. P. Craig, and S. T. Davey, "The fabrication and optical properties of Nd^{3+} in silica based optical fibers," *Mater. Lett.*, vol. 5, pp. 143-145, 1987.
[53] K. Arai, H. Namikawa, K. Kumata, T. Honda, Y. Ishii, and T. Handa, "Aluminum or phosphorus codoping effects on the fluorescence and structural properties of neodymium-doped silica glass," *J. Appl. Phys.*, vol. 59, no. 10, pp. 3430-3436, 1986.
[54] J. C. Wright, "Upconversion and excited-state energy transfer in rare-earth-doped materials," *Topics Appl. Phys.*, vol. 15, pp. 239-295, 1976.
[55] J. E. Townsend, S. B. Poole, and D. N. Payne, "Solution doping technique for fabrication of rare-earth ion doped fibers," *Electron. Lett.*, vol. 23, pp. 329-331, 1987.

[56] E. Snitzer, H. Po, F. Hakimi, R. Tumminelli, and B. C. McCollum, "Erbium fiber laser amplifier at 1.55 μm with pump at 1.49 μm and Yb sensitized Er oscillator," in *Proc. OFC* (New Orleans, LA), 1988, pap. PD-2.

[57] M. E. Fermann, D. C. Hanna, D. P. Shepherd, P. J. Suni, and J. E. Townsend, "Efficient operation of a Yb-sensitized Er fibre laser at 1.56 μm," *Electron. Lett.*, vol. 24, no. 18, pp. 1135–1136, 1988.

[58] D. C. Hanna, R. M. Percival, I. R. Perry, R. G. Smart, and A. C. Tropper, "Efficient operation of a Yb sensitized Er fiber laser pumped in the 0.8-μm region," *Electron. Lett.*, vol. 24, pp. 1068–1069, 1988.

[59] V. P. Gapontsev, S. M. Matitsin, and A. A. Sineev, "Channels of energy losses in erbium laser glasses in the stimulated emission process," *Opt. Commun.*, vol. 46, pp. 226–230, 1983.

[60] I. M. Jauncey, L. Reekie, J. E. Townsend, D. N. Payne, and C. J. Rowe, "Single longitudinal mode operation of an Nd^{3+} doped fibre laser," *Electron. Lett.*, vol. 24, pp. 24–26, 1988.

[61] T. Okoshi, K. Kikuchi, and A. Nakayama, "Novel method for high resolution measurement of laser output spectrum," *Electron. Lett.*, vol. 16, pp. 630–631, 1980.

[62] G. J. Cowle, "Laser linewidth determination by the self-heterodyne technique," Telecom Australia Res. Labs., rep. 7949, 1988.

[63] A. L. Schawlow and C. H. Townes, "Infrared and optical masers," *Phys. Rev.*, vol. 112, pp. 1940–1949, 1958.

[64] P. R. Morkel, M. C. Farries, and D. N. Payne, "Losses in fiber laser cavities," *Electron. Lett.*, vol. 24, pp. 92–93, 1988.

[65] D. C. Hanna, R. G. Smart, P. J. Suni, A. I. Ferguson, and M. W. Phillips, "Measurements of fiber laser losses via relaxation oscillations," *Opt. Commun.*, vol. 68, pp. 128–132, 1988.

[66] R. I. Laming, P. R. Morkel, D. N. Payne, and L. Reekie, "Noise in erbium-doped fiber amplifiers," in *Proc. ECOC '88* (Brighton, England), 1988, pp. 54–57.

[67] R. I. Laming, D. N. Payne, L. Reekie, and P. R. Morkel, "Erbium-doped fiber amplifiers operating at 1.5 μm," in *Proc. OCTIMA* (Rome, Italy), 1989, pp. 204–209.

[68] C. R. Giles, E. Desurvire, and J. R. Talman, "Characterization of high-speed signal amplification at $\lambda = 1.53$ μm in an erbium-doped single mode fiber," in *Proc. CLEO'88* (Los Angeles, CA), 1988, pap. PD9.

[69] T. J. Whitley and T. G. Hodgkinson, "1.54 μm Er^{3+} doped amplifier optically pumped at 807 nm," in *Proc. ECOC'88* (Brighton, England), 1988, pp. 58–61.

[70] M. J. Pettitt, R. A. Baker, and A. Hadjifotiou, "System performance of optical fibre preamplifier," *Electron. Lett.*, vol. 25, pp. 259–273, 1989.

[71] K. Hagimoto, K. Iwatsuki, A. Takada, M. Nadazawa, M. Saruwatari, K. Aida, K. Nakagawa, and M. Horiguchi, "A 212-km non-repeated transmission experiment at 1.8 Gbit/s using LD pumped Er^{3+}-doped fiber amplifiers in an IM/direct-detection repeater system," in *Proc. OFC '89* (Houston, TX), 1989, pap. PD-16.

[72] R. Olshansky, "Noise figure for erbium-doped optical fiber amplifiers," *Electron. Lett.*, vol. 24, pp. 1363–1365, 1988.

[73] P. R. Morkel and R. I. Laming, "Design considerations for the erbium-doped fiber amplifier," *Electron. Lett.*, submitted for publication.

[74] T. Mukai, Y. Yamamoto, and T. Kimura, "S/N and error-rate performance in AlGaAs semiconductor laser preamplifier and linear repeater systems," *IEEE Trans. Microwave Theory Tech.*, vol. MTT-30, pp. 1548–1556, 1982.

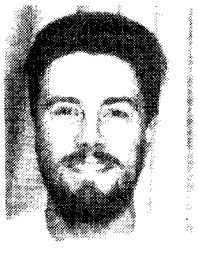

Simon B. Poole was born in Watford, England, in 1958. He received the B.Sc. degree in electrical and electronic engineering from the University of Nottingham in 1979.

In 1981, he joined the Optical Fibre Group at Southampton University as a Research Student working on optical fiber fabrication and characterization. He is now the Pirelli Research Fellow within the group. His current research interests include novel dopant materials and their uses in fiber devices.

Janet Townsend was born in Patchogue, Long Island, NY, in 1964. She received the B.Sc. degree in physics from the University of Southampton, U.K., in 1985.

Since 1985 she has been working on optical fiber fabrication and characterization in the Optical Fibre Group at the University of Southampton where she is a Research Fellow.

*

David N. Payne was born in Lewes, England, on August 13, 1944, and was educated in Central Africa. He received the B.Sc. degree in electrical engineering, the Diploma degree in quantum electronics, and the Ph.D. degree from the University of Southampton, England.

In 1972, he was appointed the Pirelli Research Fellow in the Department of Electronics, University of Southampton, and in 1977 became Senior Research Fellow. He is currently Research Reader and directs the Optical Fibre Group, consisting of some 40 members. Since 1969 his research interests have been in optical communications and have included preform and fiber fabrication techniques, optical propagation in multimode and single mode fibers, fiber and preform characterization, wavelength dispersive properties of optical fiber materials, optical-transmission measurements, and fiber devices. He has published over 100 papers and holds 11 patents. Currently, his main fields of interest are special fibers, fiber lasers and devices, fiber sensors, and optical transmission.

Dr. Payne was an Associate Editor of the JOURNAL OF LIGHTWAVE TECHNOLOGY.

*

Martin E. Fermann was born in Dubrowno, Poland, on May 9, 1960. He received the M.Sc. degree from the University of Reading, England, in 1984.

In October 1984, he joined the Optical Fibre Group at Southampton University as a Research Assistant where he is working on fiber measurements.

*

G. J. Cowle, photograph and biography not available at time of publication.

*

Richard I. Laming was born in Sheffield, England, on March 12, 1962. He received a first class honours degree in mechanical engineering from Nottingham University in 1983.

After a brief spell developing engine management systems for the Ford Motor Company Ltd. he joined the Optical Fibre Group, the University of Southampton, U.K., in October 1984, where he is now the Pirelli Research Fellow. His research interests have included fiber vibration and current sensors, while his recent work has centered on the erbium doped fiber amplifier.

Mr. Laming received in 1989 the Marconi International Fellowship, Young Scientist of the Year Award.

*

Paul Morkel was born in Malindi, Kenya, on December 9, 1961. He received the B.Sc. degree in physics from the University of Southampton, U.K., in 1983. Since 1986 he has been studying for the Ph.D. degree in the Optical Fibre Group at the University of Southampton where his interests include rare earth doped fibers and fiber resonators.

In 1983 he joined British Aerospace, Bracknell, where he worked on ring laser gyros.